Materials Today Bio 16 (2022) 100444

Contents lists available at ScienceDirect

Materials Today Bio

journal homepage: www.journals.elsevier.com/materials-today-bio

Versatile nanorobot hand biosensor for specific capture and ultrasensitive quantification of viral nanoparticles

Rui Li [a], Ya Zhao [b], Hongli Fan [a], Mingqian Chen [a], Wenjun Hu [a], Qiang Zhang [d,****], Meilin Jin [b,***], Gang L. Liu [a,**], Liping Huang [a,c,*]

[a] College of Life Science and Technology, Huazhong University of Science and Technology, Wuhan, 430074, PR China
[b] National Key Laboratory of Agricultural Microbiology, Huazhong Agricultural University, Wuhan, 430070, PR China
[c] Liangzhun (Shanghai) Industrial Co. Ltd., Shanghai, 200233, PR China
[d] College of Biomedicine and Health, Huazhong Agricultural University, Wuhan, 430070, PR China

ARTICLE INFO

Keywords:
Virus vector
Surface plasmon resonance
Biosensor
Label-free detection
Nanoparticles

ABSTRACT

Accurate determination of the concentration and viability of the viral vaccine vectors is urgently needed for preventing the spread of the viral infections, but also supporting the development and assessment of recombinant virus-vectored vaccines. Herein, we describe a nanoplasmonic biosensor with nanoscale robot hand structure (Nano RHB) for the rapid, direct, and specific capture and quantification of adenovirus particles. The nanorobot allows simple operation in practical applications, such as real-time monitoring of vaccine quantity and quality, and evaluation of vaccine viability. Modification of the Nano RHB with branched gold nanostructures allow rapid and efficient assessment of human adenovirus viability, with ultrahigh detection sensitivity of only 100 copies/mL through one-step sandwich method. Nano RHB detection results were consistent with those from the gold standard median tissue culture infectious dose and real-time polymerase chain reaction assays. Additionally, the Nano RHB platform showed high detection specificity for different types of viral vectors and pseudoviruses. Altogether, these results demonstrate that the Nano RHB platform is a promising tool for efficient and ultrasensitive assessment of vaccines and gene delivery vectors.

1. Introduction

Virus infection is an important public health issue that can harbor significant economic and social burdens, as it became widely recognized by the rapid global spread of the coronavirus disease 2019 (COVID-19) [1,2]. This issue can be tackled by fast and accurate virus detection [3–5], while the establishment of herd immunity through vaccination can effectively prevent the spread of the virus [6,7]. Recombinant vector-vaccines based on viral vectors are highly valued for their potential use in vaccine development and disease prevention applications. Among them, adenovirus-based vector vaccines, which are immunogenic and relatively safe in humans, can be produced quickly and inexpensively [8,9]. During the recent COVID-19 pandemic, adenoviruses have become an ideal vaccine vector for preventing infection, severe illness, and death [10,11]. Nevertheless, an infectiously active viral vaccine is required so it can enter the body to induce an immune response and establish immune memory [12,13]. Moreover, accurate determination of the concentration of the viral vaccine vectors is very important for production quality control and correct vaccine administration [14,15]. Therefore, a detection strategy for broad applicability that can quantitatively assess viral particles [16], but can also rapidly determine the viral viability without any sample pretreatment is still warranted [17,18].

Microbiology techniques, namely plaque assays, are the "gold standard" to study infectious diseases and diagnose viruses [19]. Plaque assay is the most accurate method for virus viability detection but it requires several days to grow plaques and virus in host cells, and rely on the ability of different viruses to replicate in cell culture systems, which increases the time and labor-intensive costs for result validation [20]. Quantitative polymerase chain reaction (qPCR) detection of viral nucleic acids is also widely used for highly sensitivity, quantitative virus

* Corresponding authors. College of Life Science and Technology, Huazhong University of Science and Technology, Wuhan, 430074, PR China.
** Corresponding author.
*** Corresponding authors.
**** Corresponding author.
E-mail addresses: zhangq_0401@mail.hzau.edu.cn (Q. Zhang), jml8328@126.com (M. Jin), loganliu@hust.edu.cn (G.L. Liu), lphuang@aliyun.com (L. Huang).

https://doi.org/10.1016/j.mtbio.2022.100444
Received 14 July 2022; Received in revised form 24 September 2022; Accepted 27 September 2022
Available online 28 September 2022
2590-0064/© 2022 Published by Elsevier Ltd. This is an open access article under the CC BY-NC-ND license (http://creativecommons.org/licenses/by-nc-nd/4.0/).

detection [21]. However, this approach requires strict environmental requirements and expensive laboratory instruments, all of which limit its output speed and clinical availability. Although immunofluorescence and immunodiagnostic assays that use antigens directly improve detection time [22], they lack sensitivity and accuracy. Surface plasmon resonance (SPR), which has emerged as a suitable and reliable platform in non-destructive testing, has the advantages of being label-free, maintaining molecular activity, and to provide real-time kinetics when detecting intermolecular interactions [23,24]. However, the traditional SPR technology uses two-dimensional planar chips, which requires a complex and precise prism optical system to capture weak signals; thus, its optical sensitivity is limited [25,26]. In turn, nanoarray surface plasmon resonance (NanoSPR) is a highly sensitive three-dimensional (3D) structure sensor that can track analytes near its surface without disturbing distant molecules within the solution, which makes the NanoSPR sensor suitable for detecting complex samples including cell supernatants, serum, among others [27,28]. Moreover, our previous research demonstrated that uniform nanocup structures allow NanoSPR biosensors to have unique optical properties, which makes them a benchtop, easy-to-use detection instrument that can meet personal and laboratory requirements. However, this planar NanoSPR-based biosensing systems [29,30] for label-free detection of molecules and nanoparticles still needs to be improved by integrating more efficient surface capturing functional nanostructures.

In this study, we designed a multi-metal-layer NanoSPR chip (comprising titanium, silver, and gold) with unique additional surface nanostructures. More specifically, we created a novel nanoplasmon sensor with nanorobot hand (Nano RHB) integration that is expected to function as a virus capturing platform for one-step rapid quantification of vector viruses and efficient large-scale assessment of virus viability (Fig. 1a and b). This Nano RHB platform displays great potential for quality control for vaccine and delivery vector research and production, and was used for label-free and high-throughput detection of human adenovirus within 5 min without requiring signal amplification and washing procedures (Fig. 1c). Furthermore, Nano RHB integrated with gold nanoparticles (AuNPs), achieved using freeze-drying technology, was shown to detect ultra-low virus concentrations by one-step sandwich method, with a limit of detection (LOD) of 100 copies/mL (Fig. 1d). Taken together, this platform allows simple operation in practical applications, real-time monitoring of vaccine quantity and quality, and evaluation of vaccine viability, thereby representing a convenient and rapid evaluation method to monitor and accurately detect viral vectors.

2. Experimental section

2.1. Materials

Hydrogen tetrachloroaurate (III) trihydrate ($HAuCl_4 \cdot 3H_2O$, 99.9%), hexylsilane, bovine serum albumin (BSA), polyethylene glycol thiol (PEG, Mw = 20,000), and phosphate-buffered saline (PBS) were purchased from Sigma-Aldrich (St. Louis, MO, USA). Dopamine (99%) and tris(hydroxymethyl)methyl aminomethane (Tris, 99.9%) were purchased from Aladdin Technology Co, Ltd. (Hong Kong, China). Anti-adenovirus hexon protein antibody (ab252760) was purchased from Abcam (Cambridge, UK). Factor X protein (11,076-H08B) was purchased from Sino Biological Inc. (Beijing, China). *GFP*-specific primers were synthesized by Tsingke Biotechnology Co, Ltd. (Beijing, China) (forward, 5′–TATATCATGGCCGACAAGCAGAAG–3′ and reverse, 5′–CTGGGT GCTCAGGTAGTGGTTGT–3′). All chemicals were used without further purification.

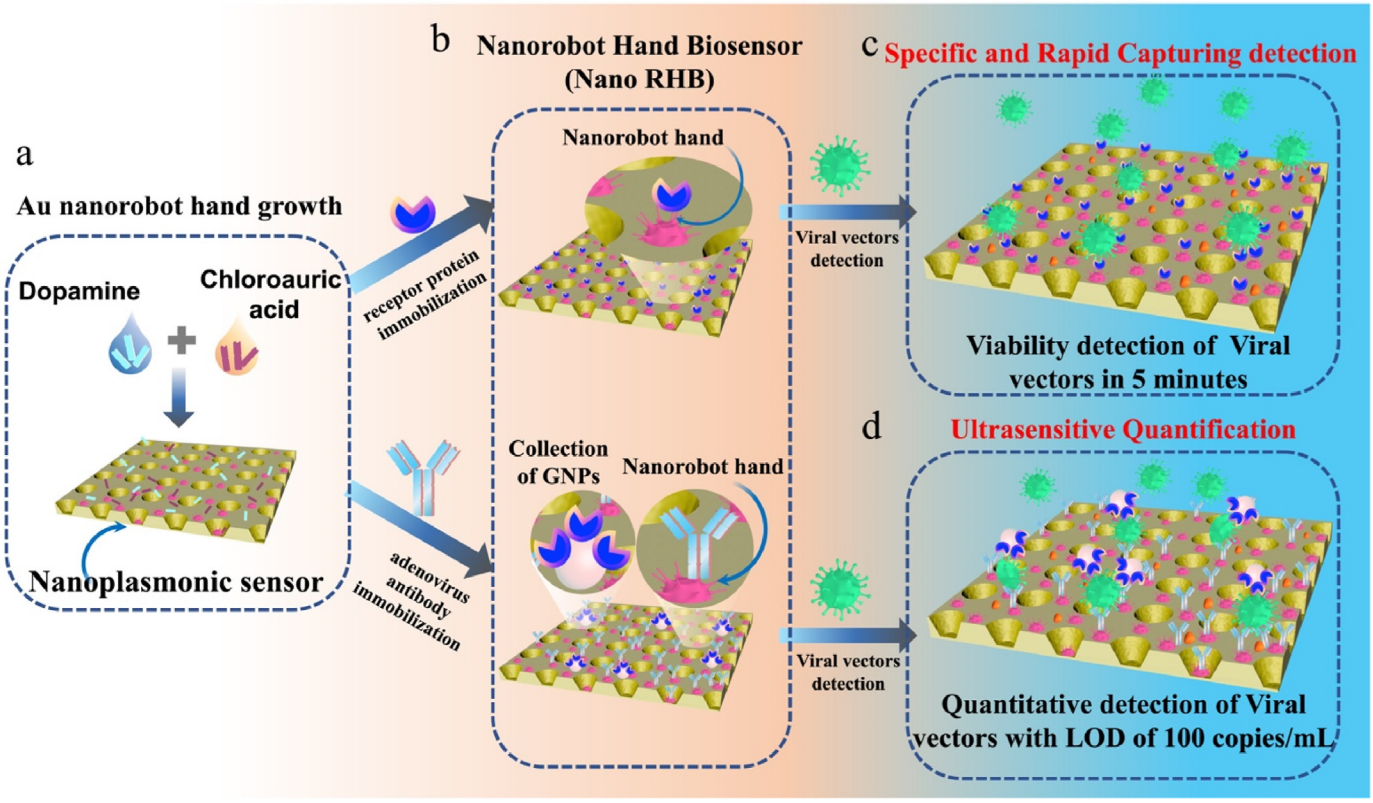

Fig. 1. One-step rapid quantification of viral particles using the Nano RHB platform. a) NanoSPR sensor modified by highly sensitive nanorobot hands. b) Scheme of the NanoSPR sensor immobilized receptor protein or antibody to form a NanoRHB platform with specific capture ability. c) Schematics of the minute-time scale of the Nano RHB platform for detecting viral vectors within 5 min. d) Schematics of the ultra-sensitivity scale of the Nano RHB platform for detecting viral vectors using one-step sandwich method within 15 min.

2.2. Production and purification of recombinant CAR protein

The nucleotide sequence of the extracellular active region with a signal peptide of the coxsackie adenovirus receptor (CAR) was synthesized by Tsingke Biotechnology Co, Ltd. and cloned into a pCMV-mFc expression vector. Recombinant plasmid was transfected into 293 F cells grown in serum-free medium (SFM4HEK293; Cytiva, Marlborough, MA, USA) after 4 days of cell culture. The supernatant was collected by clarification filtration, and the protein was purified using AKTA Pure 25 with PrismA protein A and Superdax200 increase column (Cytiva). The specificity and purity of the CAR recombinante protein was examined by sodium dodecyl-sulfate polyacrylamide gel electrophoresis (SDS-PAGE) (Fig. S1). Protein concentrations were determined using a bicinchoninic acid assay (BCA) kit and the samples were stored at −80 °C.

2.3. Cells and cell cultures

HEK293 cell line was cultured in complete Dulbecco's modified Eagle's medium (Cytiva) containing 10% fetal bovine serum (Gibco; Thermo Fisher Scientific, Waltham, MA, USA). 293 A and 293 T cells were incubated at 37 °C in 5% CO_2, and 293 F cells were grown in serum-free medium (SFM4HEK293; Cytiva) at 37 °C in a humidified 8% CO_2 incubator rotating at 150 rpm.

2.4. Packaging of recombinant GFP adenovirus

HEK293A cells were transfected with *Pac*I-linearized pDC316-EGFP and pBHGloxdeltaE13Cre plasmids in Lip8000 DNA transfection solution (Beyotime, Shanghai, China). Adenovirus plaques and green fluorescence became visible 9 days post-transfection, and the recombinant adenoviruses were serially passaged in HEK293 cells when full cytopathic effect was observed. The virus was harvested via plaque purification. Cells were frozen and thawed three times (temperature range: −20 to 37 °C), and the cell precipitates were removed by centrifugation at 12,000 rpm for 10 min, and the virus samples were stored at −80 °C. Viral titers [reported as 50% tissue culture infectious dose ($TCID_{50}$/mL)] were calculated using the Reed–Muench method with 293 A cells.

2.5. Preparation of AuNPs and AuNP-labeled FX protein or CAR protein

The traditional colloidal gold reduction method was adopted for the synthesis of colloidal Au particles. Briefly, sodium citrate reducing agent was added to a chloroauric acid solution to reduce the gold ions to gold atoms. Then, the following steps were followed: 100 mL of 0.01% $HAlCl_4$ solution was heated and boiled, and 1 mL of 1% sodium citrate was quickly added to the solution and continued to boil for 5 min. The solution turned orange-red, and 30-nm AuNPs were obtained.

To label AuNPs with factor X (FX) proteins or CAR proteins, it was necessary to adjust the pH value of the colloidal AuNP solution to produce a suitable environment for the coupling of the protein [31]. Thus, 0.1 mM K_2CO_3 was added to 1.5 mL of colloidal AuNPs to achieve a pH of 8. Then, 8 μL of FX protein (2.11 mg/mL) or CAR protein (0.6 mg/mL) was added to the colloidal AuNPs solution and incubated for 15 min. After adding 22.5 μL of blocking solution (10 mM PBS + 10% PEG 2 W) for 15 min, the FX/CAR protein-labeled colloidal AuNPs suspension was centrifuged at 8,000 rpm for 15 min. The supernatant of the centrifuge tube was discarded, and the pellet was resuspended in 270 μL of stabilization buffer (20 mM Tris [pH 9.2] + 0.5% sucrose) and stored at 4 °C until use.

2.6. Fabrication of Ti–Ag–Au nanoplasmonic sensor chip

The nanoplasmonic array sensor chip was prepared using a replication molding method. The original model was a silicon wafer with 100 nm radius and 450 nm depth that was prepared by photolithography and using plasma corrosion technique. It was repeatedly arranged at a period of 420 nm. The hydrophobicity of the mold was ensured before replication by placing it in a vacuum dryer filled with hexylsilane for 10 h. Then, an ultra-violate curable polymer or an optical adhesive was evenly applied to the mold with the nanocup structure, and a polyethylene terephthalate (PET) sheet was placed on top of it. After 3 min exposure to ultraviolet irradiation, the PET sheet with the nanocup array structure was peeled off and was deposited with 10 nm titanium (Ti), 70 nm silver (Ag), and 10 nm gold (Au) in an electron beam evaporator. The film was cut into the same size as the bottom of a 96-well plate (length = 128 mm, width = 85.2 mm, height = 16.2 mm) printed with a Objet30 Prime printer (Stratasys Ltd, Rehovot, Israel), and glued to the bottom of the sensor plate.

2.7. Surface functionalization with robot hand structure

Using the seed growth method on the chip surface it may be possible to enhance the surface plasmon effect. Here, we propose the use of *in situ* dopamine deposition to modulate the surface strain of growing seeds for the direct synthesis of highly branched Au superparticles [32,33]. We evaluated a range of dopamine and chloroauric acid (0.2–1.5 mM) solutions in Tris-HCl buffer. The specific process was as follows: 11 μL of dopamine and 10 μL of chloroauric acid were added to 1 mL of 8 mM Tris-HCL solution. Then, 150 μL of this solution was placed into each well of the chip plate and incubated in the dark at an analysis temperature of 25 °C for 45 min. After washing the chip twice with deionized water, 2.5 μL of 10 μg/mL CAR/FX protein carbonate buffer solution was added to the center of the chip well using a spotter, and the solution was incubated in a 50 °C oven for 1.5 h. Then, the chip wells were rinsed twice with deionized water and blocked with 50 μL of blocking agent (1% BSA + PBS with Tween 20 [PBST]) for 30 min at 37 °C. After discarding the liquid in the wells, the surface-modified chip plate was stored at 4 °C until further use.

2.8. Virus particles detection using Nano RHB platform

We demonstrated the feasibility of the platform by quantitatively detecting adenoviruses. Adenovirus samples to be tested (detection range from 2.5×10^4 to 1.6×10^6 $TCID_{50}$/mL) were diluted 10-fold with a solution of 10 mM PBS, 0.8% sucrose, 2.5% PEG 2 W, and 0.5% DMSO, and added to the modified nanoplasmonic 96-well plate sensor. The initial full spectrum optical density (OD) of the reaction was read using an Epoch 2 microplate reader (Biotek, Winoosk, VT, USA). After 5 min of reaction at 700 rpm on a shaker at 37 °C, the full spectrum OD value at the end of the reaction was immediately read. Simple data processing of OD-final value reduce OD-initial value was used to quantify the specific number of adenoviruses.

2.9. Virus particles detection using AuNP-coupled Nano RHB platform

To further improve the sensitivity of the Nano RHB platform, the CAR-labeled AuNPs were assembled on the chip by physical freeze-drying technology. A transferpettor (BrandTech Scientific, Inc, Essex, CT, USA) was used to add 5 μL of the reconstituted CAR-labeled AuNP solution onto the surface of the chip fixed with FX protein. The Nano RHB chip was placed at −80 °C for 1 h, then in a vacuum drying box (Yiheng, Shanghai, China) to dry for 5 min, and finally in a vacuum-sealed bag containing a desiccant. For virus detection, the bag was unpacked and 30 μL of adenovirus samples of different concentrations (detection range: 0.39–1,600 $TCID_{50}$/mL) were added to the well of the sensor. A microplate reader was then used to read the full spectrum of at the starting point. The chip was then reacted at 37 °C on a shaker for 15 min, and a universal microplate reader was used to detect and read the full spectrum at the end point.

2.10. Virus particles detection using qPCR

Viral genomic DNA of recombinant adenovirus-GFP was extracted using TGuide S32 Automatic nucleic acid extractor (Tiangen, Beijing, China) with a MagicPure 96 Viral DNA/RNA Kit (Trans, Beijing, China). Fragment amplification was performed using the Taq Pro Universal SYBR qPCR Master Mix (Vazyme, Nanjing, China) for qPCR. Then, qPCR was performed to quantify the DNA copies of the virus using the Applied Biosystems QuantStudio 6Flex Real-Time PCR System (Thermo Fisher Scientific). The amount of DNA obtained of the target *GFP* gene was normalized to a standard curve designed using a plasmid containing the full-length *GFP* (pEGFP-N1; 4,733 bp).

2.11. Statistical analysis

Data were analyzed using Origin 8.0 software (Origin Lab Corporation, Northampton, MA, USA). All data is presented as mean ± standard deviation (SD). The statistical comparison between groups was performed following the student's *t*-test (two-tailed). *$p < 0.01$, **$p < 0.001$ and ***$p < 0.0001$.

3. Results and discussion

3.1. Detection principle of adenovirus detection using the Nano RHB platform

The adenovirus capturing platform with one-step rapid quantitative detection was developed based on a label-free NanoSPR biosensor with extraordinary optical transmission (EOT) effect, which can be excited by unpolarized light and does not require complex optical devices [24,34,35]. In this study, we designed a novel multifunctional NanoSPR biosensor with nanorobot hands by implementing the gold seed growth method directly on the nanocup array chip. Owing their special nanocup structures as seed templates, different shapes of branched gold nanostructures were produced on the surface of the chip via polydopamine molecules. These branched gold nanostructures can function similarly to smart robot hands, thereby enhancing the SPR resonance effect to improve the sensitivity of the chip, but also increasing the surface area to improve the chip encapsulation efficiency (Fig. 1). Integrating these ultrasensitive biosensors into standard 96-well or 32-well plates enables direct monitoring of dynamic binding curves and quantitative detection of adenoviral vectors or vaccines using microsamples.

The principle of the versatile Nano RHB platform for virus capture strategy was based on the specific binding properties of ligands and receptors. First, the recombinant human CAR, FX protein, or anti-adenovirus hexon protein antibody, which can bind to the fiber protein (spikes extruding on the virus capsid) and hexon protein (the major capsid protein) of adenoviruses, respectively, were immobilized on the surface of the Nano RHB. During the label-free reaction of the direct detection, the adenovirus was expected to bind to the coating proteins. Thus, with increasing concentrations of adenovirus, the SPR effects of the Nano RHB would be enhanced. Moreover, changes in the OD of the Nano RHB at specific wavelengths, which are proportional to adenovirus concentrations, could be monitored using a general microplate reader.

Previous studies showed that AuNPs can significantly improve the detection sensitivity of nanoplasmonic biosensors. Therefore, we innovatively implemented a rapid one-step, no-wash sandwich assay for the quantitative detection of adenovirus using a protein-labeled integrated AuNP-coupled Nano RHB platform. In this system, the protein-labeled AuNPs were physically assembled to the protein/antibody-modified Nano RHB using the vacuum drying method. When the diluted samples were placed onto the Nano RHB wells, the protein-labeled AuNPs on chip surface reach free state in a few seconds and their protein markers bind specifically to adenovirus. The adenovirus and protein-labeled AuNPs complexes were simultaneously captured by the immobilized protein or antibody of the chip platform to form sandwich immunoconjugated particles (protein AuNP-adenovirus-protein/antibody). These final particles would then generate an enhanced signal change and further improve the detection sensitivity of the Nano RHB platform.

3.2. Characterization of the NanoSPR sensor chip and AuNPs

In this study, a novel plasmonic nanocup array sensor chip was fabricated with multi-layer metal structure by considering the stability and favorable SPR effect of the sensor. Compared with the use of single-structure noble metal systems, the use of multi-layer metal composite nanostructures can further improve the local electric field enhancement effect, which has great potential for sensitive detection [36,37]. Here, the periodic nanocup periodicity, depth, and radius was 420, 450, and 100 nm, respectively. The titanium, silver, and gold layers from bottom to top were 10, 70, and 10 nm thick. The image of the 12-inch NanoSPR sensor chip with the multicolor light effect represents the high uniformity of the chip sensor (Fig. 2a). The chip was cut and pasted to an open-bottom 96-well plate (Fig. 2b) or 16-well plate (Fig. 2c) to generate high-throughput detection devices for adenovirus. A 32-well plate was specifically designed by combining two 16-well plates fixed on the plate holder (Fig. S2). Next, the refractive index (RI) of the NanoSPR sensor considering different solutions was measured, as it reflects the detection sensitivity of the sensor [38]. The microscope observation of the sensor chip surface in both reflection and transmission (Fig. 2d) showed distinctly different colors in media with different RI values, including air (RI = 1.0), 10% glucose (RI = 1.35), and 10% PBST (RI = 1.40), further indicating that the sensor chip exhibited high detection sensitivity. The nanostructure of the chip and AuNPs were characterized by scanning electron microscopy (SEM). Overall, the size of each nanocup structure showed a high degree of homogeneity (Fig. 2e), and the cross-sectional view of the chip showed that the nanocup pores were 450 nm deep and uniformly arranged (Fig. 2f). The average diameter of the synthesized AuNPs was approximately 30 nm (Fig. 2g).

3.3. Optimizing surface-grown Au NanoRobot hands of NanoSPR chips

Considerable progress has been made in the exploration of nanostructures such as nanoparticles, nanorods, and nanopores that are uniformly arranged on plasmonic biochemical sensors, and the results have been applied to the detection of biological samples [39,40]. Importantly, modifications of the chip can lead to better repeatability of transmission and reflection spectra, which can be helpful to obtain high-performance plasmonic biosensors [41]. Indeed, modification of SPR biosensors using AuNPs can be performed through physical electrostatic interactions or chemical linkages (for example, through amino [42] and thiol [43] groups). The main principle of physical electrostatic adsorption is to directly immerse the gold film of the sensor in a solution of AuNPs. Despite its simple operation and low cost, the physical electrostatic adsorption process has the limitations of poor adsorption and instability. Therefore, we applied the method of generating chemical bonds in an innovative way to grow 3D gold nanobranches on gold nanostructure chips and form island-in-cup structures. We directly synthesized highly branched gold superparticles on the surface of the NanoSPR chip sensor and modulated the surface of gold seeds using dopamine. The subsequently generated gold seeds were then continuously adsorbed, thereby enhancing the EOT of the sensor [44]. This signal-like SPR confinement of the electromagnetic field around the edge of the nanocup can be an effective sensing site that uses fast decay lengths and even lead to flow-through sensing, improving detection sensitivity.

We screened several dopamine and chloroauric acid concentrations (0.1–1.5 mM) to determine the optimal chip modification conditions. According to SEM images of the NanoSPR chips, 3D gold nanobranches of different shapes and sizes were grown on the chip surface as the concentration of dopamine and chloroauric acid increased (Fig. 3a). Moreover, NanoSPR chips treated with different concentrations of dopamine and chloroauric acid showed different surface colors, changing from light

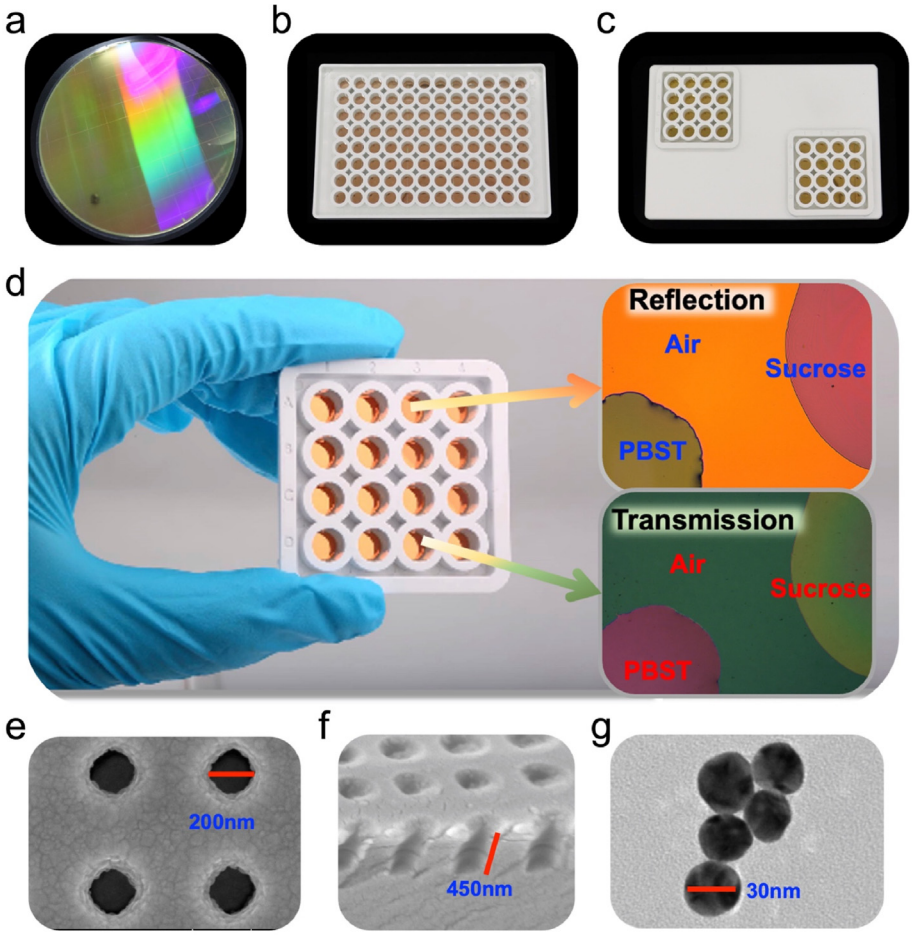

Fig. 2. Characteristics of the NanoSPR chip and AuNPs. a) Photograph of 12-inch Ti–Ag–Au NanoSPR chip. b) Integration of the Ti–Ag–Au NanoSPR chip with a standard 96-well plate. c) Integration of the NanoSPR chip with two 16-well plates. d) Photograph of a 16-well chip plate and microscope images of NanoSPR chip with two drops of PBST and sucrose solution on the chip surface. e–g) Scanning electron microscope images of repeating nanocup array with 200 nm diameter and f) 450 nm height, and of g) AuNPs with 30 nm diameter.

green to dark green, then to red (Fig. 3a). To further evaluate the optical response sensitivity of the Nano RHB modified with the island-in-cup structure, the absorption spectra of the chip in 5% sucrose (1.339) solution (Fig. 3b) and its difference compared with the spectra of the chip in 5% sucrose and in water (1.333) were measured (Fig. S3). The relative OD value of the Au nanobranch modified chip at 590 and 570 nm was calculated using the differential spectrum of 5% sucrose solution and water, and the sensitivity of the modified chip was preliminarily evaluated (Fig. 3c and Fig. S3). The results showed that a gradual increase of the relative OD value varied within 0.264–0.405, as dopamine and chloroauric acid concentrations increased from 0 to 0.6 mM, and a significant decrease of the relative OD value varied within 0.405–0.128, as dopamine and chloroauric acid concentrations increased from 0.6 to 1.5 mM. Hence, 3D gold nanohands merged on the sensor surface may produce more scattering, which makes the resonant spectrum of the sensor wider than that of the unmodified sensor. The relative change in OD reached the highest point (0.405) when the concentration of both dopamine and chloroauric acid was 0.6 mM. Compared with the reaction signal of the bare chip under the same conditions, the reaction signal of the chip modified with the gold nanobranch showed 0.15 amplification and a 60% increase in sensitivity. Using atomic force microscopy, we were able to characterize the structure and uniformity of the nanorobot hand more vividly. Fig. 3d shows a 3D image of the chip without any modification and demonstrates that the surface of the chip was relatively smooth. Under the optimal modification condition (0.6 mM), many bumps could be observed evenly distributed on the surface of the chip (Fig. 3e). Figs. S5(a) and (b), respectively, present the two-dimensional structure of the chip with or without nanorobot hands on its surface as determined by Atomic force microscopy.

Consequently, the concentration of both dopamine and chloroauric acid at 0.6 mM was selected as the modification concentration used for subsequent experiments. Nevertheless, owing to the changes in the roughness and charge of the chip surface, the efficiency of protein immobilization can also be further improved.

3.4. Quick capture and accurate quantification of adenovirus using the label-free Nano RHB CAR sensor platform

Most adenoviruses enter cells after binding to CAR, and the fiber (spikes on the viral capsid) and hexon proteins (the main capsid protein) are the main determinants of cell neutralization [45]. Therefore, real-time data, such as virus titer, recovery rate, and function, can be analyzed by targeting to the fiber or hexon proteins of adenoviruses to obtain high-quality viral vectors.

After the gold nanobranch reaction, a small amount of dopamine solution remaining on the modified chip surface can form a dopamine polymerized film to improve the adsorption efficiency of proteins on the chip surface. To verify the detection capability of the Nano RHB platform, CAR proteins were first anchored to the super surface of the nanobranch chip to directly capture adenoviruses and detect their viral infectivity within 5 min (Fig. 4a). The original absorption spectra of the adjacent sensor modification steps exhibited an obvious change (Fig. S6). The differential spectra of different concentrations of adenovirus (2.5×10^4 to 1.6×10^6 $TCID_{50}$/mL) showed that the light intensity decreased at approximately 570 nm and increased at 590 nm with an increase in the adenovirus concentration (Fig. 4b). However, no change was observed concerning the differential spectrum of the serum dilution solution without adenovirus that served as control. Fig. 4c shows that a four-

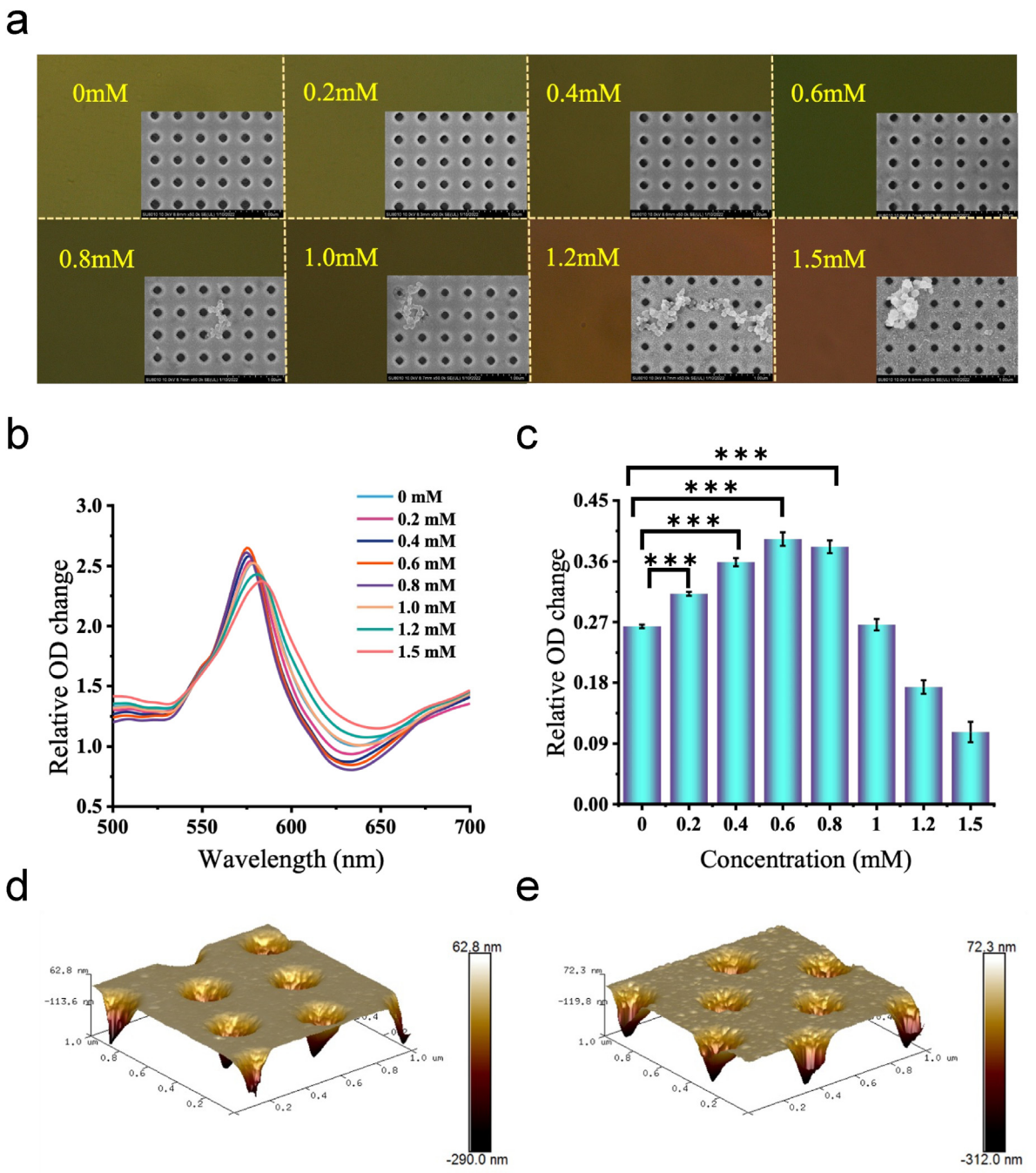

Fig. 3. a) Microscopic images and SEM images of the NanoSPR chip modified with L-cysteine and chloroauric acid at 0.2–1.5 mM. b) Measurement of the absorption spectral changes of the NanoSPR chip in water and in 5% sucrose after the chip was modified with a range of dopamine and chloroauric acid concentrations (0.2–1.5 mM). c) Relative OD changes at 590 and 570 nm after surface modification of the sensor chip. Data are shown as mean ± SD ($n = 3$). The statistical comparison between groups was performed following the student's *t*-test (two-tailed). *p < 0.01, **p < 0.001 and ***p < 0.0001. d,e) Atomic force microscopy image of the (d) unmodified NanoSPR chip and (e) NanoSPR chip under the optimal modification condition.

parameter fit of the two-wavelength OD differential values at 590 and 570 nm for each concentration yielded a correlation coefficient (R^2) of 0.996. The LOD for adenovirus was 2.5×10^4 $TCID_{50}$/mL using the Nano RHB CAR platform. The two-wavelength OD changes ($OD_{590}-OD_{570}$) of different concentrations of adenovirus were monitored in real-time to investigate the dynamic binding curves between the Nano RHB and the adenoviruses within 4 min. As shown in Fig. 4d, the negative control sample was almost in a horizontal state, whereas the two-wavelength OD differential values of the adenovirus groups showed a positive increase as the concentration of adenovirus increased. If the chip is placed in a vacuum-sealed bag containing a desiccant, it can be stored in a harsh environment for a long time. Moreover, protein degeneration or degradation within the reagent can be prevented during transportation, which likely increases the accuracy of detection. Noteworthily, the Nano RHB device tested with three standard positive samples exhibited good stability when stored at different temperatures and for different time periods (Fig. 4e).

3.5. Quick capture and accurate quantification of adenovirus using the label-free Nano RHB FX sensor platform

Adenoviruses include three important structural proteins, namely

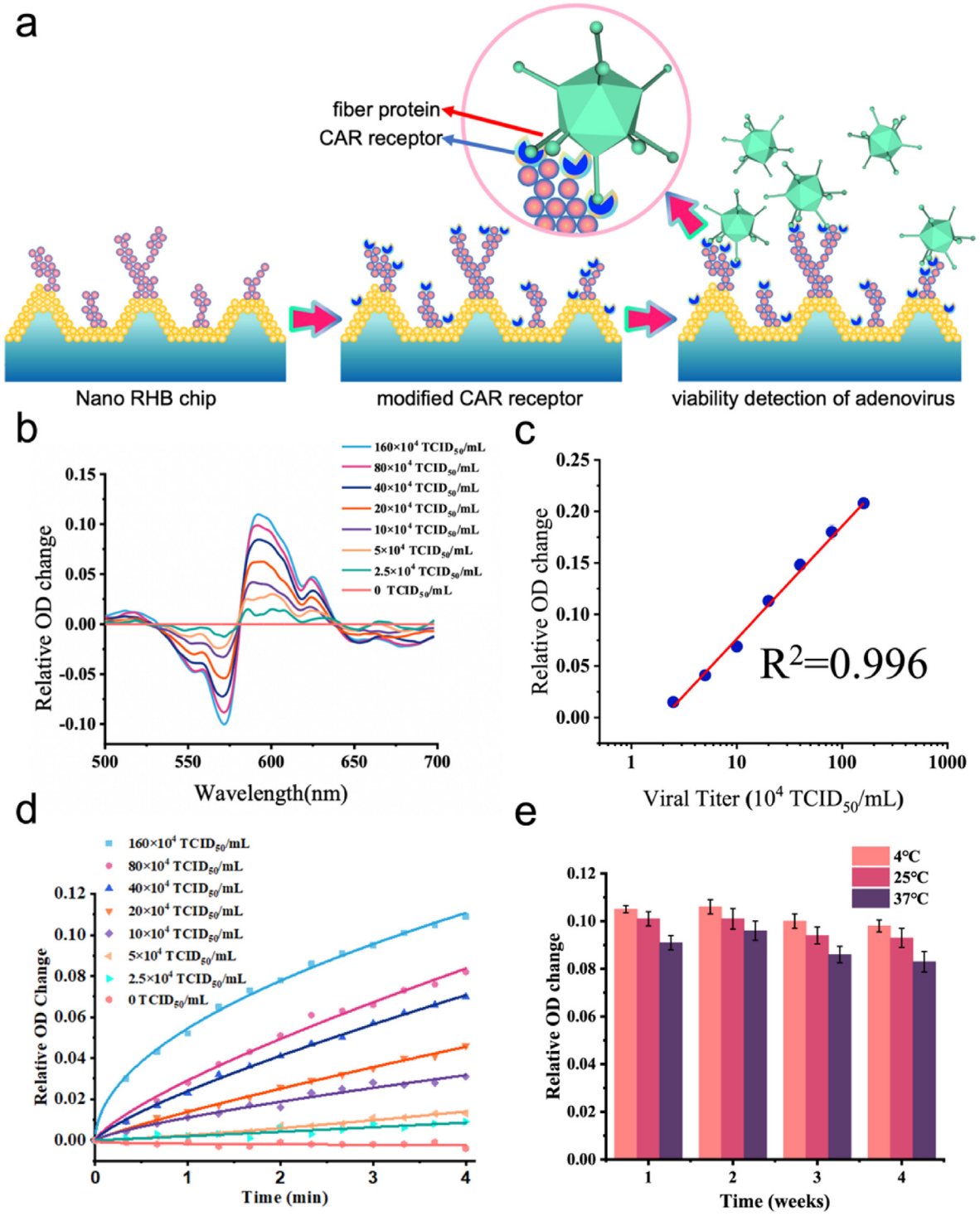

Fig. 4. Label-free detection of adenovirus using a CAR-coated Nano RHB platform within 5 min. a) Schematic diagram of adenovirus recognition based on the CAR-coated Nano RHB platform. b) Absorption differential spectra at 500–700 nm using the CAR-coated Nano RHB assay for adenovirus detection in the concentration ranges of 2.5×10^4 to 1.6×10^6 $TCID_{50}$/mL. c) Standard curve of the CAR-coated Nano RHB for adenovirus detection ($R^2 = 0.996$). d) Kinetic binding curves of adenovirus at the OD difference values ($OD_{590}-OD_{570}$) based on the CAR-coated Nano RHB, with a detection range of 2.5×10^4 to 1.6×10^6 $TCID_{50}$/mL. e) Stability of the Nano RHB at different storage temperatures and time periods were tested using three standard positive samples. Data are shown as mean ± SD ($n = 3$).

pentonbase, hexon, and fiber. It has been shown that FX can bind to the adenovirus hexon protein and target the virus to hepatocytes [46]. Therefore, adenovirus hexon protein concentration can be directly detected using the FX receptor. Herein, the FX-coated Nano RHB chip was used to demonstrate the detection generality of the Nano RHB platform for adenovirus assay (Fig. 5a). Adenovirus samples in the same concentration range as above described were added to different chip wells, and the absorption differential spectra of different samples showed a change similar to that of the CAR-coated Nano RHB chip at 5 min (Fig. 5b). In addition, fitting the dual-wavelength OD differential values at different concentrations resulted in a curve with a correlation coefficient (R^2) of 0.990 and LOD of 2.5×10^4 $TCID_{50}$/mL (Fig. 5c). Although

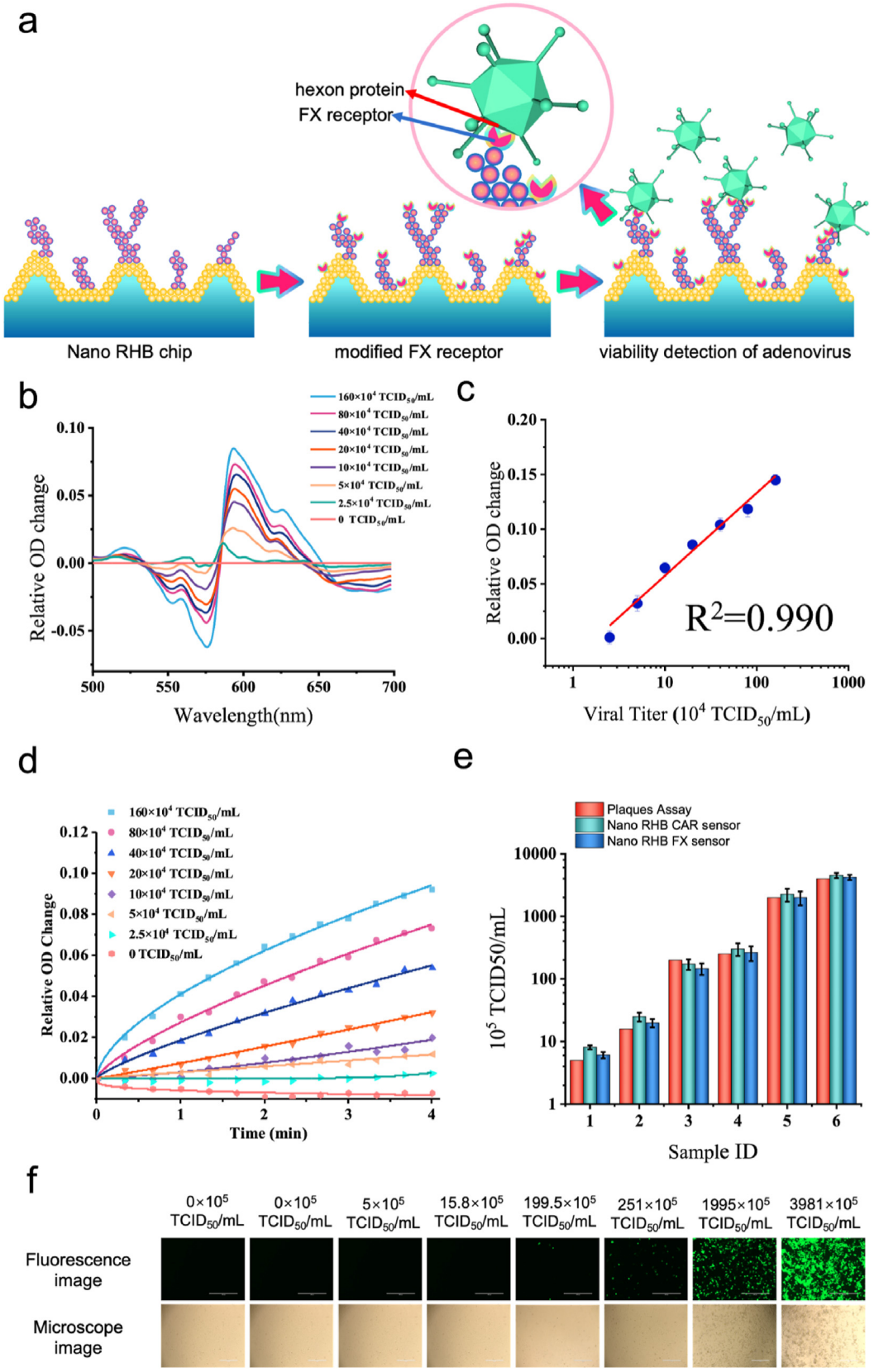

Fig. 5. Label-free detection of adenovirus using the FX-modified NanoSPR platform. a) Schematic of adenovirus captured by the FX-coated Nano RHB. b) Differential spectra at 500–700 nm of the FX-coated Nano RHB for adenovirus detection with different concentrations (2.5×10^4–1.6×10^6 $TCID_{50}$/mL). c) Two-wavelength OD differential value change of the Nano RHB at 570 and 590 nm regarding different adenovirus concentrations ($R^2 = 0.990$). d) Kinetic binding curves of the FX-coated Nano RHB at the OD difference values ($OD_{590}-OD_{570}$)for adenovirus detection with different concentrations (2.5×10^4–1.6×10^6 $TCID_{50}$/mL). e) Comparison of CAR- and FX-modified Nano RHB platform assays and adenovirus titers assay for six adenovirus samples. Data are shown as mean ± SD ($n = 3$). f) Fluorescence and bright field images of transfected cells at day 9 post-transfection.

the two-wavelength OD differential value at 590 and 570 nm were weaker than that of the CAR-coated Nano RHB chip, the distinctly different concentration binding curves illustrated the superiority of the Nano RHB platform for adenovirus detection (Fig. 5d).

Since the Nano RHB platform captured and quantified the adenovirus viability based on the specific binding properties between ligands and receptors, the concentration of adenovirus detected by Nano RHB may be more relevant to the virus infection titer results. Therefore, the virus viability of six samples was used for comparative validation of the Nano RHB platform *vs.* the Reed–Muench method, which can be used to calculate the $TCID_{50}$. As shown in Fig. 5e, the two-wavelength OD difference values obtained from CAR- and FX-modified Nano RHB platform assays, respectively, were positively correlated with the virus titers (plaques assay). In addition, the fluorescence became weaker when an adenovirus concentration of 10^7 $TCID_{50}$/mL was co-cultured with cells (Fig. 5f), whereas the Nano RHB platform could detect the adenovirus titer of 2.5×10^4 $TCID_{50}$/mL within 5 min. Hence, these results demonstrated that the multifunctional Nano RHB Sensor is likely to create a rapid one-step and high-throughput adenovirus quantitative detection platform with higher detection efficiency and sensitivity that gold-standard methods. Compared with the conventional NanoSPR detection of adenovirus, the Nano RHB platform with gold nano-branching showed significantly improved sensitivity (Fig. S7).

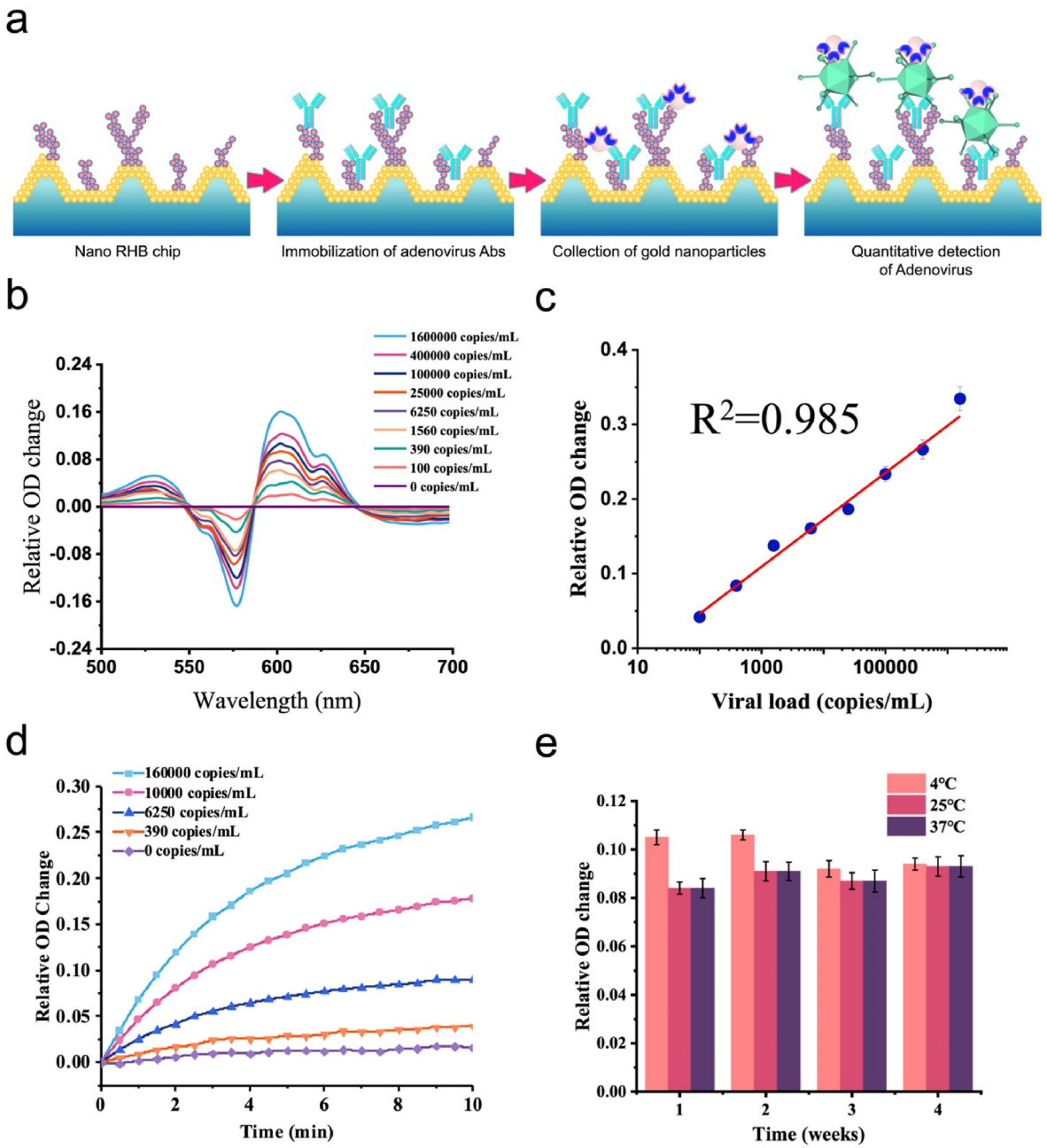

Fig. 6. Label-free detection of total adenovirus with AuNP-enhanced nanoplasmonic virus capture platform. a) Schematic diagram of the nanoplasmonic virus capture platform integrated with AuNPs for detection of adenoviruses. b) Absorption spectrum of adenovirus at 500–700 nm, with a detection range of 1×10^2–1.6×10^6 copies/mL. c) Standard curve for adenovirus ($R^2 = 0.985$). d) Kinetic binding curve of adenovirus determined at the OD difference values ($OD_{600}-OD_{580}$) using an anti-adenovirus antibody-coated microarray, with a detection range of 1×10^2–1.6×10^6copies/mL. e) Stability of the Nano RHB platform integrated with AuNPs at different storage temperatures and time periods using three standard positive samples. Data are shown as mean ± SD ($n = 3$).

3.6. One-step and wash-free ultrasensitive detection of adenovirus using the Nano RHB platform

To further improve the detection sensitivity and expand the detection application field of the developed Nano RHB platform, we established a rapid and wash-free sandwich assay method for the ultrasensitive detection of adenovirus by directly integrating the detection protein-labeled AuNPs onto the capture antibody-modified Nano RHB platform. The traditional sandwich method is a common qualitative and quantitative detection approach that has several steps, including capture antibody immobilization, antigen analyte detection, washing, addition of another paired detection antibody, washing, and analysis. To simplify this complicated washing process and shorten the total detection time [47,48], physical immobilization between the AuNPs and Nano RHB devices was performed by lyophilization. Based on this developed Nano RHB platform, we demonstrated that the one-step sandwich technique had no non-specific binding between the complex samples and the sensors (Fig. S8). In contrast, when samples were added into the Nano RHB wells, protein-labeled AuNPs could rapidly bind to the adenoviruses and form protein-virus-protein sandwich particles (Fig. 6a and S9a) [49].

After several protein-pairing comparison experiments, CAR immobilized on the Nano RHB chip as the capture protein and FX-labeled AuNPs as the detection protein achieved the more robust replicability and detection sensitivity within 15 min (Figs. S9 and S10). CAR–CAR, FX–CAR, and CAR–FX showed the optional pair results. However, when the coat protein was replaced with antibodies with higher affinity for the adenovirus, the sensitivity of the platform was further improved. As shown in Fig. 6a–b, the optimal resonant wavelength of the Nano RHB was red-shifted to 600 and 580 nm when combined with AuNPs [33] and the relative OD value decreased at 580 nm and increased at 600 nm with increasing adenovirus concentrations (1×10^2–1.6×10^6 copies/mL). SEM images of the test chip after capturing the adenovirus particles showed that many AuNPs could specifically bind to the nanostructure surface of the functionalized Nano RHB platform (Fig. S11). The standard curve of the two-wavelength OD difference values relative to the adenovirus concentrations yielded an R^2 of 0.985 (Fig. 6c). The LOD for

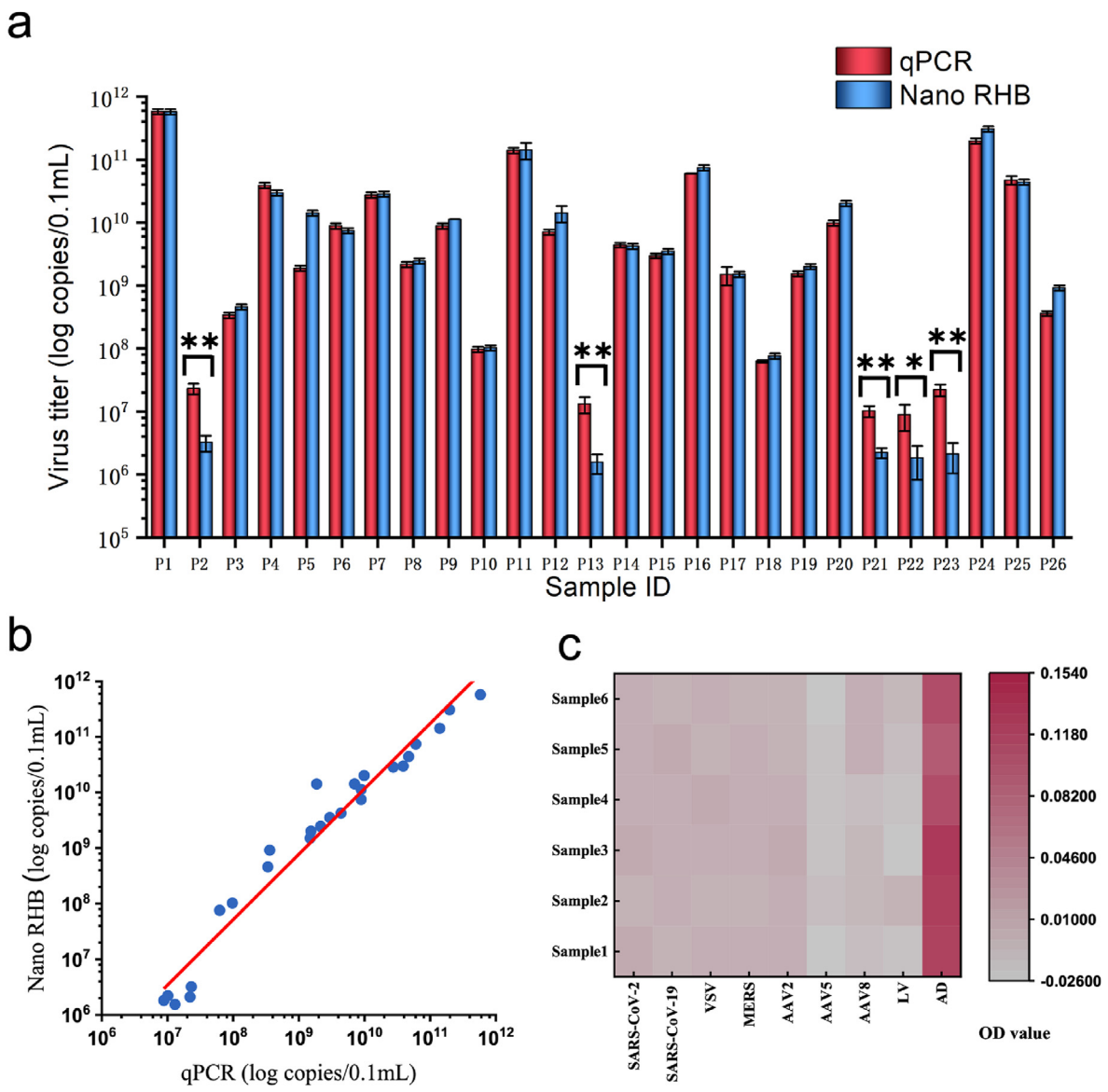

Fig. 7. Comparison of the detection outcome for adenovirus of the Nano RHB platform with that of other detection methods. a) Comparison of qPCR assay and Nano RHB platform to quantify the concentration of adenovirus. Data are shown as mean ± SD ($n = 3$). The statistical comparison between groups was performed following the student's *t*-test (two-tailed). *$p < 0.01$, and **$p < 0.001$. b) Curve fitting of the qPCR and Nano RHB assays for adenovirus quantification detection. c) Specificity of the Nano RHB platform for the detection adenovirus as compared with four other pseudoviruses and four viral vectors.

adenovirus was estimated at 100 copies/mL using the sandwich method based on the Nano RHB platform, which enabled a ~10,000-fold increase in detection sensitivity. The dynamic binding curves of different concentrations of the adenovirus were also detected in real-time at the resonance wavelengths of 580 and 600 nm (Fig. 6d). The relative two-wavelength OD changes (OD_{600}–OD_{580}) were positively correlated with the adenovirus concentrations, whereas the dynamic curve of the adenovirus-free group showed almost no change. Similarly, the two-wavelength OD difference values (OD_{600}–OD_{580}) were obtained from the dynamic curves at 10 min.

For gene therapy and vaccine development, accurate quantification of adenovirus vectors and detection accuracy of living indicators are important, but the assessment of viral vector effectiveness remains challenging. The one-step Nano RHB platform has ultra-fast detection speed, and ultra-high sensitivity and effectiveness, which greatly reduces the workload of experimenters when analyzing large numbers of vaccinated serum samples, thereby improving the efficiency of the evaluation process and facilitating the determination of the effects of gene therapy and vector vaccines. Four positive and four negative samples were randomly selected for experimental verification, and there was no non-specific binding reaction with the AuNP-integrated chip; the results show the difference between negative and positive samples (Fig. S8). As shown in Fig. 6e, the Nano RHB platform prepared by lyophilization technology exhibited good stability under different storage conditions. These data suggest that the Nano RHB platform can be used for nanomaterial-enhanced one-step sandwich detection method.

3.7. Accuracy and specificity verification of Nano RHB for detecting adenovirus

To confirm the detection accuracy of the Nano RHB platform, we collected 26 adenovirus cell supernatant samples with African swine fever genes for blind comparison. Both the developed Nano RHB assay and the gold standard qPCR method were used to quantify the concentrations of the adenovirus. Owing to the very low bulk effect of the Nano RHB chip, the cell supernatant samples could only be diluted and directly added into the chip wells for detection without non-specific reactions. As shown in Fig. 7a and b, the detection results obtained with the Nano RHB platform were very close to those of the qPCR, which reveals a strong correlation between the two assays ($R^2 = 0.970$). However, there are differences in the detection results of the two detection methods for the low concentration of 5 samples, such as P2, P13, P21, P22 and P23. This phenomenon may be due to the poor virus activity caused by repeated freezing and thawing of samples in the refrigerator. This result further proved that the developed Nano RHB platform was more suitable for quantitative detection of intact virus particles. Conventional qPCR detection required 2 h of work, whereas Nano RHB detected the adenovirus within 5 min for high-concentration samples and 15 min for very low-concentration samples. Furthermore, the Nano RHB technology was compatible with a wide range of sample types, allowing the direct detection of complex samples using small sample amounts without additional processing.

To further evaluate the specificity of Nano RHB, adenovirus, four pseudoviruses (SARS-CoV-2 virus, SARS, MERS, and VSV), and four viral vectors (three adeno-associated viruses [AAV-2, AAV-5, and AAV-8] and one lentivirus [LV-3]) were simultaneously evaluated. Significant positivity was observed only in adenovirus samples, with no signal changes for the other eight pseudoviruses and viral vectors (Fig. 7c). These results demonstrated the agreement between the Nano RHB platform technology and the two currently used detection methods, revealing the robust performance of our Nano RHB.

4. Conclusion

We developed a nanoplasmonic virus capturing platform for the rapid detection of adenovirus viability and concentration by exploiting specific epitope−CAR/FX protein interactions. Dopamine and chloroauric acid were added to the surface of the NanoSPR chip well to grow nanorobot hands with greater virus capturing efficiency and detection sensitivity than the bare sensor. The receptor protein or monoclonal antibody was immobilized to form a highly specific nanoplasmonic virus capturing sensor, and the detection result was obtained within only 5 min. In addition, using lyophilization technology to integrate CAR-labeled AuNPs on the monoclonal antibody-modified Nano RHB platform, the detection sensitivity could be further increased by 5-fold, making it an ultra-sensitive platform. The unique SPR effect of the AuNP-coupled Nano RHB enabled highly sensitive and rapid adenovirus detection in one-step sandwich method without requiring washing steps and complex sample pre-treatment. Applying the platform to 26 cell supernatant samples showed excellent agreement with the results of the traditional qPCR and fluorescence image titration assays. Nano RHB assays significantly shortened the total detection time from days and hours to minute-time scale, and improved the testing capacity by directly binding to the viral surface protein to simultaneously and rapidly detect virus viability and concentration. Indeed, Nano RHB platform improved the testing capacity to simultaneous high-throughput detection of up to 96 samples with 5 min, which was better and faster than the traditional SPR assay [50]. Moreover, the detection sensitivity of the Nano RHB platform was 0.34 $TCID_{50}$/mL, which was much higher than that of adenovirus detection by SPR (14.3 $TCID_{50}$/mL) [50]. Compared with the label-free SPR technology of Biacore (Cytiva, USA), the detection of adenovirus using a CAR sensor ranged from 0.11×10^9 to 14×10^9 virus particles/mL, with an estimated LOD of 0.11×10^9 virus particles/mL, which was much lower than that of our Nano RHB assay (100 copies/mL). These results demonstrated that the Nano RHB platform has the potential to be a high-throughput and multifunctional device for rapid quality control of viral vector-vaccines on a large scale, as well as for other viral vectors-based assays.

Author Contributions

Rui Li: Conceptualization, Methodology, Investigation, Data curation, Visualization, and Writing – original draft. **Ya Zhao**: Investigation. **Hongli Fan**: Data acquisition. **Mingqian Chen**: Software. **Wenjun Hu**: Supervision. **Qiang Zhang**: Supervision, and Funding acquisition. **Meilin Jin**: Supervision, Funding acquisition, and Project administration. **Gang L. Liu**: Supervision, Funding acquisition, and Project administration. **Liping Huang**: Supervision, Writing – review & editing, and Project administration.

The data that support the findings of this study are available from the corresponding author upon reasonable request.

Declaration of competing interest

The authors declare that they have no known competing financial interests or personal relationships that could have appeared to influence the work reported in this paper.

Data availability

Data will be made available on request.

Acknowledgments

Rui Li, Ya Zhao, Hongli Fan contributed equally to this work. This work was supported by a grant from the National Natural Science Foundation of China (91959107, 82072735), the National Key R&D Plan of China (2020YFC0861900), the Fundamental Research Funds for the Central Universities (2019kfyXMPY002, 2020kfyXGYJ111), the Fundamental Research Funds for the Central Universities (2021XXJS112) and the Hubei Science and Technology Major Project (2021ACB0004).

Abbreviations

CAR	coxsackie adenovirus receptor
FX	factor X
LOD	limit of detection
NanoSPR	nanoplasmonic biosensors
OD	optical density
qPCR	quantitative polymerase chain reaction
RI	refractive indices
SEM	scanning electron microscopy
SPR	surface plasmon resonance
$TCID_{50}$	median tissue culture infectious dose

Appendix B. Supplementary data

Supplementary data to this article can be found online at https://doi.org/10.1016/j.mtbio.2022.100444.

Appendix A. Supplementary data

Supplementary data to this article can be found online at http://

References

[1] N. Chen, M. Zhou, X. Dong, J. Qu, F. Gong, Y. Han, Y. Qiu, J. Wang, Y. Liu, Y. Wei, J.a. Xia, T. Yu, X. Zhang, L. Zhang, Epidemiological and clinical characteristics of 99 cases of 2019 novel coronavirus pneumonia in wuhan, China: a descriptive study, Lancet 395 (2020) 507–513, https://doi.org/10.1016/S0140-6736(20)30211-7.

[2] M.U.G. Kraemer, C.-H. Yang, B. Gutierrez, C.-H. Wu, B. Klein, D.M. Pigott, L.d. Plessis, N.R. Faria, R. Li, W.P. Hanage, J.S. Brownstein, M. Layan, A. Vespignani, H. Tian, C. Dye, O.G. Pybus, S.V. Scarpino, The effect of human mobility and control measures on the covid-19 epidemic in China, Science 368 (2020) 493–497, https://doi.org/10.1126/science.abb4218.

[3] L. Coughlan, E.J. Kremer, D.M. Shayakhmetov, Adenovirus-based vaccines – a platform for pandemic preparedness against emerging viral pathogens, Mol. Ther. (2022), https://doi.org/10.1016/j.ymthe.2022.01.034.

[4] S. Afkhami, M.R. D'Agostino, A. Zhang, H.D. Stacey, A. Marzok, A. Kang, R. Singh, J. Bavananthasivam, G. Ye, X. Luo, F. Wang, J.C. Ang, A. Zganiacz, U. Sankar, N. Kazhdan, J.F.E. Koenig, A. Phelps, S.F. Gameiro, S. Tang, M. Jordana, Y. Wan, K.L. Mossman, M. Jeyanathan, A. Gillgrass, M.F.C. Medina, F. Smaill, B.D. Lichty, M.S. Miller, Z. Xing, Respiratory Mucosal Delivery of Next-Generation Covid-19 Vaccine Provides Robust Protection against Both Ancestral and Variant Strains of Sars-Cov-2, Cell, 2022, https://doi.org/10.1016/j.cell.2022.02.005.

[5] S. Capone, A. Raggioli, M. Gentile, S. Battella, A. Lahm, A. Sommella, A.M. Contino, R.A. Urbanowicz, R. Scala, F. Barra, A. Leuzzi, E. Lilli, G. Miselli, A. Noto, M. Ferraiuolo, F. Talotta, T. Tsoleridis, C. Castilletti, G. Matusali, F. Colavita, D. Lapa, S. Meschi, M. Capobianchi, M. Soriani, A. Folgori, J.K. Ball, S. Colloca, A. Vitelli, Immunogenicity of a new gorilla adenovirus vaccine candidate for covid-19, Mol. Ther. 29 (2021) 2412–2423, https://doi.org/10.1016/j.ymthe.2021.04.022.

[6] M. Jeyanathan, S. Afkhami, F. Smaill, M.S. Miller, B.D. Lichty, Z. Xing, Immunological considerations for covid-19 vaccine strategies, Nat. Rev. Immunol. 20 (2020) 615–632, https://doi.org/10.1038/s41577-020-00434-6.

[7] J.S. Heitmann, T. Bilich, C. Tandler, A. Nelde, Y. Maringer, M. Marconato, J. Reusch, S. Jäger, M. Denk, M. Richter, L. Anton, L.M. Weber, M. Roerden, J. Bauer, J. Rieth, M. Wacker, S. Hörber, A. Peter, C. Meisner, I. Fischer, M.W. Löffler, J. Karbach, E. Jäger, R. Klein, H.-G. Rammensee, H.R. Salih, J.S. Walz, A covid-19 peptide vaccine for the induction of sars-cov-2 t cell immunity, Nature 601 (2022) 617–622, https://doi.org/10.1038/s41586-021-04232-5.

[8] C. Chéneau, E.J. Kremer, Adenovirus-extracellular protein interactions and their impact on innate immune responses by human mononuclear phagocytes, Viruses 12 (2020), https://doi.org/10.3390/v12121351.

[9] C. Chéneau, K. Eichholz, T.H. Tran, T.T.P. Tran, O. Paris, C. Henriquet, J.J. Bajramovic, M. Pugniere, E.J. Kremer, Lactoferrin retargets human adenoviruses to tlr4 to induce an abortive nlrp3-associated pyroptotic response in human phagocytes, Front. Immunol. 12 (2021), 685218, https://doi.org/10.3389/fimmu.2021.685218.

[10] R.B. Kennedy, Efficacy of an adenovirus type 5 vectored sars-cov-2 vaccine, Lancet 399 (2022) 212–213, https://doi.org/10.1016/S0140-6736(21)02834-8.

[11] S.A. Halperin, L. Ye, D. MacKinnon-Cameron, B. Smith, P.E. Cahn, G.M. Ruiz-Palacios, A. Ikram, F. Lanas, M. Lourdes Guerrero, S.R. Muñoz Navarro, O. Sued, D.A. Lioznov, V. Dzutseva, G. Parveen, F. Zhu, L. Leppan, J.M. Langley, L. Barreto, J. Gou, T. Zhu, H. Mao, L. Gagnon, S.-P. Tran, S.T. Khan, A.G. Becerra Aquino, E.E. Saldaña Montemayor, N.E. Rivera Martínez, V.C. Bohórquez López, J.A. Simón Campos, F.d.J. Pineda Cárdenas, W. Chen, L. Hou, Z. Zhang, G. Corral, E. López, R. Teijeiro, M.F. Alzogaray, C. Zaidman, G. Lopardo, B. Goecke, R.M. Feijooó Seoane, S.F. Mahmood, E.A. Khan, J. Akram, S. Abbas, N. Salahuddin, E. Rozhkova, T. Zubkova, Final efficacy analysis, interim safety analysis, and immunogenicity of a single dose of recombinant novel coronavirus vaccine (adenovirus type 5 vector) in adults 18 years and older: an international, multicentre, randomised, double-blinded, placebo-controlled phase 3 trial, Lancet 399 (2022) 237–248, https://doi.org/10.1016/S0140-6736(21)02753-7.

[12] R. Weissleder, H. Lee, J. Ko, M.J. Pittet, Covid-19 diagnostics in context, Sci. Transl. Med. 12 (2020), https://doi.org/10.1126/scitranslmed.abc1931 eabc1931.

[13] F.-C. Zhu, Y.-H. Li, X.-H. Guan, L.-H. Hou, W.-J. Wang, J.-X. Li, S.-P. Wu, B.-S. Wang, Z. Wang, L. Wang, S.-Y. Jia, H.-D. Jiang, L. Wang, T. Jiang, Y. Hu, J.-B. Gou, S.-B. Xu, J.-J. Xu, X.-W. Wang, W. Wang, W. Chen, Safety, tolerability, and immunogenicity of a recombinant adenovirus type-5 vectored covid-19 vaccine: a dose-escalation, open-label, non-randomised, first-in-human trial, Lancet 395 (2020) 1845–1854, https://doi.org/10.1016/S0140-6736(20)31208-3.

[14] Q. Mao, M. Xu, Q. He, C. Li, S. Meng, Y. Wang, B. Cui, Z. Liang, J. Wang, Covid-19 vaccines: progress and understanding on quality control and evaluation, signal transduction and targeted therapy, 199, 2021. https://doi.org/10.1038/s41392-021-00621-4.

[15] C. Scheller, F. Krebs, R. Minkner, I. Astner, M. Gil-Moles, H. Wätzig, Physicochemical properties of sars-cov-2 for drug targeting, virus inactivation and attenuation, vaccine formulation and quality control, Electrophoresis 41 (2020) 1137–1151, https://doi.org/10.1002/elps.202000121.

[16] D. Jacot, G. Greub, K. Jaton, O. Opota, Viral load of sars-cov-2 across patients and compared to other respiratory viruses, Microb. Infect. 22 (2020) 617–621, https://doi.org/10.1016/j.micinf.2020.08.004.

[17] Detailed protocol for the novel and scalable viral vector upstream process for aav gene therapy manufacturing, Hum. Gene Ther. 32 (2021) 850–861, https://doi.org/10.1089/hum.2020.054.

[18] A.S. Peinetti, R.J. Lake, W. Cong, L. Cooper, Y. Wu, Y. Ma, G.T. Pawel, M.E. Toimil-Molares, C. Trautmann, L. Rong, B. Mariñas, O. Azzaroni, Y. Lu, Direct detection of human adenovirus or sars-cov-2 with ability to inform infectivity using DNA aptamer-nanopore sensors, Sci. Adv. 7 (2021), eabh2848, https://doi.org/10.1126/sciadv.abh2848.

[19] Y. Takumi-Tanimukai, S. Yamamoto, N. Ogasawara, S. Nakabayashi, K. Mizuta, K. Yamamoto, R. Miyata, T. Kakuki, S. Jitsukawa, T. Sato, H. Tsutsumi, T. Kojima, K. Takano, S.-i. Yokota, A hydroxypropyl methylcellulose plaque assay for human respiratory syncytial virus, J. Virol Methods 304 (2022), 114528, https://doi.org/10.1016/j.jviromet.2022.114528.

[20] K. Pehler-Harrington, M. Khanna, C.R. Waters, K.J. Henrickson, Rapid detection and identification of human adenovirus species by adenoplex, a multiplex pcr-enzyme hybridization assay, J. Clin. Microbiol. 42 (2004) 4072–4076, https://doi.org/10.1128/JCM.42.9.4072-4076.2004.

[21] A.S. Peinetti, R.J. Lake, W. Cong, L. Cooper, Y. Wu, Y. Ma, G.T. Pawel, M.E. Toimil-Molares, C. Trautmann, L. Rong, B. Mariñas, O. Azzaroni, Y. Lu, Direct detection of human adenovirus or sars-cov-2 with ability to inform infectivity using DNA aptamer-nanopore sensors, Sci. Adv. 7 (2021), eabh2848, https://doi.org/10.1126/sciadv.abh2848.

[22] M. Zhang, X. Li, J. Pan, Y. Zhang, L. Zhang, C. Wang, X. Yan, X. Liu, G. Lu, Ultrasensitive detection of sars-cov-2 spike protein in untreated saliva using sers-based biosensor, Biosens. Bioelectron. 190 (2021), 113421, https://doi.org/10.1016/j.bios.2021.113421.

[23] N. Bellassai, R. D'Agata, V. Jungbluth, G. Spoto, Surface plasmon resonance for biomarker detection: advances in non-invasive cancer diagnosis, Front. Chem. 7 (2019) 570, https://doi.org/10.3389/fchem.2019.00570.

[24] M. Soler, C.S. Huertas, L.M. Lechuga, Label-free plasmonic biosensors for point-of-care diagnostics: a review, Expert Rev. Mol. Diagn. 19 (2019) 71–81, https://doi.org/10.1080/14737159.2019.1554435.

[25] K. Takemura, Surface plasmon resonance (spr)- and localized spr (lspr)-based virus sensing systems: optical vibration of nano- and micro-metallic materials for the development of next-generation virus detection technology, Biosensors 11 (2021) 250, https://doi.org/10.3390/bios11080250.

[26] A. Belushkin, F. Yesilkoy, H. Altug, Nanoparticle-enhanced plasmonic biosensor for digital biomarker detection in a microarray, ACS Nano 12 (2018) 4453–4461, https://doi.org/10.1021/acsnano.8b00519.

[27] H. Kurt, P. Pishva, Z.S. Pehlivan, E.G. Arsoy, Q. Saleem, M.K. Bayazıt, M. Yüce, Nanoplasmonic biosensors: theory, structure, design, and review of recent applications, Anal. Chim. Acta 1185 (2021), 338842, https://doi.org/10.1016/j.aca.2021.338842.

[28] E. Mauriz, P. Dey, L.M. Lechuga, Advances in nanoplasmonic biosensors for clinical applications, Analyst 144 (2019) 7105–7129, https://doi.org/10.1039/c9an00701f.

[29] L. Huang, L. Ding, J. Zhou, S. Chen, G.L. Liu, One-step rapid quantification of sars-cov-2 virus particles via low-cost nanoplasmonic sensors in generic microplate reader and point-of-care device, Biosens. Bioelectron. 171 (2021), 112685, https://doi.org/10.1016/j.bios.2020.112685.

[30] T. Dang, W. Hu, W. Zhang, Z. Song, G.L. Liu, Protein binding kinetics quantification via coupled plasmonic-photonic resonance nanosensors in generic microplate reader, Biosens. Bioelectron. 142 (2019), 111494, https://doi.org/10.1016/j.bios.2019.111494.

[31] K. Lee, H. Lee, K.H. Bae, T.G. Park, Heparin immobilized gold nanoparticles for targeted detection and apoptotic death of metastatic cancer cells, Biomaterials 31 (2010) 6530–6536, https://doi.org/10.1016/j.biomaterials.2010.04.046.

[32] Q. Zhong, J. Feng, B. Jiang, Y. Fan, Q. Zhang, J. Chen, Y. Yin, Strain-modulated seeded growth of highly branched black au superparticles for efficient photothermal conversion, J. Am. Chem. Soc. 143 (2021) 20513–20523, https://doi.org/10.1021/jacs.1c11242.

[33] L. Huang, Y. Li, C. Luo, Y. Chen, N. Touil, H.-E. Annaz, S. Zeng, T. Dang, J. Liang, W. Hu, H. Xu, J. Tu, L. Wang, Y. Shen, G.L. Liu, Novel nanostructure-coupled biosensor platform for one-step high-throughput quantification of serum

neutralizing antibody after covid-19 vaccination, Biosens. Bioelectron. 199 (2022), 113868, https://doi.org/10.1016/j.bios.2021.113868.
[34] P. Jia, D. Kong, H. Ebendorff-Heidepriem, Flexible plasmonic tapes with nanohole and nanoparticle arrays for refractometric and strain sensing, ACS Appl. Nano Mater. 3 (2020) 8242–8246, https://doi.org/10.1021/acsanm.0c01673.
[35] P. Jia, H. Jiang, J. Sabarinathan, J. Yang, Plasmonic nanohole array sensors fabricated by template transfer with improved optical performance, Nanotechnology 24 (2013), 195501, https://doi.org/10.1088/0957-4484/24/19/195501.
[36] Y. Lei, W. Zhao, Y. Zhang, Q. Jiang, J.-H. He, A. Baeumner, Z. Wang, K. Salama, H. Alshareef, A mxene-based wearable biosensor system for high-performance in vitro perspiration analysis, Small 15 (2019), 1901190, https://doi.org/10.1002/smll.201901190.
[37] R.J. Westerwaal, J.S.A. Rooijmans, L. Leclercq, D.G. Gheorghe, T. Radeva, L. Mooij, T. Mak, L. Polak, M. Slaman, B. Dam, T. Rasing, Nanostructured pd–au based fiber optic sensors for probing hydrogen concentrations in gas mixtures, Int. J. Hydrogen Energy 38 (2013) 4201–4212, https://doi.org/10.1016/j.ijhydene.2012.12.146.
[38] T. Dang, W. Hu, W. Zhang, Z. Song, Y. Wang, M. Chen, H. Xu, G.L. Liu, Protein binding kinetics quantification via coupled plasmonic-photonic resonance nanosensors in generic microplate reader, Biosens. Bioelectron. 142 (2019), 111494, https://doi.org/10.1016/j.bios.2019.111494.
[39] Y. Sun, Y. Xia, Increased sensitivity of surface plasmon resonance of gold nanoshells compared to that of gold solid colloids in response to environmental changes, Anal. Chem. 74 (2002) 5297–5305, https://doi.org/10.1021/ac0258352.
[40] Y. Kalachyova, D. Mares, V. Jerabek, K. Zaruba, P. Ulbrich, L. Lapcak, V. Svorcik, O. Lyutakov, The effect of silver grating and nanoparticles grafting for lsp–spp coupling and sers response intensification, J. Phys. Chem. C 120 (2016) 10569–10577, https://doi.org/10.1021/acs.jpcc.6b01587.
[41] J. Bao, X. Qiu, H. Yang, W. Lu, M. Yang, W. Gu, L. Wu, D. Huo, Y. Luo, C. Hou, Disposable 3d gnas/aunps DNA-circuit strip for mirnas dynamic quantification, Small 16 (2020), e2001416, https://doi.org/10.1002/smll.202001416.
[42] H.-M. Kim, D. Hong Jeong, H.-Y. Lee, J.-H. Park, S.-K. Lee, Improved stability of gold nanoparticles on the optical fiber and their application to refractive index sensor based on localized surface plasmon resonance, Opt Laser. Technol. 114 (2019) 171–178, https://doi.org/10.1016/j.optlastec.2019.02.002.
[43] S. Shi, L. Wang, R. Su, B. Liu, R. Huang, W. Qi, Z. He, A polydopamine-modified optical fiber spr biosensor using electroless-plated gold films for immunoassays, Biosens. Bioelectron. 74 (2015) 454–460, https://doi.org/10.1016/j.bios.2015.06.080.
[44] O. Tokel, F. Inci, U. Demirci, Advances in plasmonic technologies for point of care applications, Chem. Rev. 114 (2014) 5728–5752, https://doi.org/10.1021/cr4000623.
[45] P.W. Roelvink, A. Lizonova, J.G.M. Lee, Y. Li, J.M. Bergelson, R.W. Finberg, D.E. Brough, I. Kovesdi, T.J. Wickham, The coxsackievirus-adenovirus receptor protein can function as a cellular attachment protein for adenovirus serotypes from subgroups a, c, d, e, and f, J. Virol. 72 (1998) 7909–7915, https://doi.org/10.1128/JVI.72.10.7909-7915.1998.
[46] C.Y. Chen, S.M. May, M.A. Barry, Targeting adenoviruses with factor x-single-chain antibody fusion proteins, Hum. Gene Ther. 21 (2010) 739–749, https://doi.org/10.1089/hum.2009.190.
[47] A.R. Patel, Functional and engineered colloids from edible materials for emerging applications in designing the food of the future, Adv. Funct. Mater. 30 (2018), https://doi.org/10.1002/adfm.201806809.
[48] M.A. Hamaly, S.R. Abulateefeh, K.M. Al-Qaoud, A.M. Alkilany, Freeze-drying of monoclonal antibody-conjugated gold nanorods: colloidal stability and biological activity, Int. J. Pharm. 550 (2018) 269–277, https://doi.org/10.1016/j.ijpharm.2018.08.045.
[49] B. Yu, J. Woo, M. Kong, D.M. O'Carroll, Mode-specific study of nanoparticle-mediated optical interactions in an absorber/metal thin film system, Nanoscale 7 (2015) 13196–13206, https://doi.org/10.1039/C5NR02217G.
[50] P.N. Abadian, N. Yildirim, A.Z. Gu, E.D. Goluch, Spri-based adenovirus detection using a surrogate antibody method, Biosens. Bioelectron. 74 (2015) 808–814, https://doi.org/10.1016/j.bios.2015.07.047.